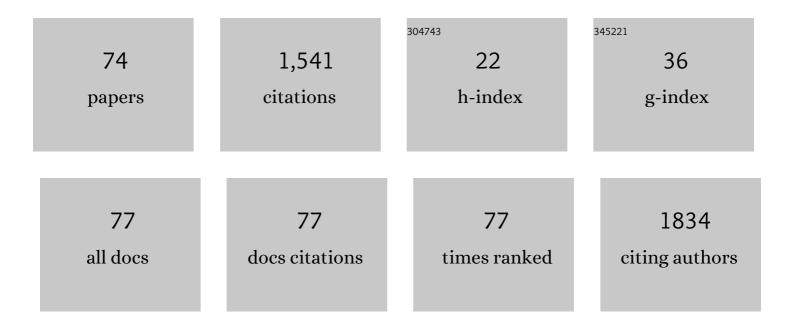
List of Publications by Year in descending order

Source: https://exaly.com/author-pdf/6179874/publications.pdf Version: 2024-02-01



#	Article	IF	CITATIONS
1	Hydrothermal synthesis and characterization of aluminium and sulfate substituted 1.1nm tobermorites. Journal of Alloys and Compounds, 2009, 467, 332-337.	5.5	118
2	FTIR spectroscopic, thermal and XRD characterization of hydroxyapatite from new natural sources. Spectrochimica Acta - Part A: Molecular and Biomolecular Spectroscopy, 2011, 83, 56-60.	3.9	110
3	Numerical description of photoelectric absorption coefficients for fundamental parameter programs. X-Ray Spectrometry, 2003, 32, 442-451.	1.4	90
4	Direct Z-scheme of Cu2O/TiO2 enhanced self-cleaning, antibacterial activity, and UV protection of cotton fiber under sunlight. Applied Surface Science, 2019, 479, 953-962.	6.1	90
5	Classical univariate calibration and partial least squares for quantitative analysis of brass samples by laser-induced breakdown spectroscopy. Spectrochimica Acta, Part B: Atomic Spectroscopy, 2010, 65, 658-663.	2.9	59
6	Hydrothermal synthesis and characterizations of Ti substituted Mn-ferrites. Journal of Alloys and Compounds, 2012, 529, 29-33.	5.5	52
7	Spectroscopic investigation of PM2.5 collected at industrial, residential and traffic sites in Taif, Saudi Arabia. Journal of Aerosol Science, 2015, 79, 97-108.	3.8	46
8	On the elemental composition of PM _{2.5} in central Cairo, Egypt. X-Ray Spectrometry, 2013, 42, 276-283.	1.4	45
9	Cathodically activated Au/TiO2 nanocomposite synthesized by a new facile solvothermal method: An efficient electrocatalyst with Pt-like activity for hydrogen generation. Electrochimica Acta, 2018, 290, 404-418.	5.2	45
10	Method development and optimization for the determination of selenium in bean and soil samples using hydride generation electrothermal atomic absorption spectrometry. Talanta, 2011, 85, 1350-1356.	5.5	42
11	Utilization of standardless analysis algorithms using WDXRF and XRD for Egyptian iron ore identification. X-Ray Spectrometry, 2012, 41, 355-362.	1.4	38
12	Elemental Composition of PM2.5 Particles Sampled in Industrial and Residential Areas of Taif, Saudi Arabia. Aerosol and Air Quality Research, 2013, 13, 1356-1364.	2.1	38
13	Method development for the determination of Cd, Cu, Ni and Pb in PM2.5 particles sampled in industrial and urban areas of Greater Cairo, Egypt, using high-resolution continuum source graphite furnace atomic absorption spectrometry. Microchemical Journal, 2014, 113, 4-9.	4.5	37
14	Removal of COOH, Cd and Pb using water hyacinth: FTIR and flame atomic absorption study. Journal of the Iranian Chemical Society, 2009, 6, 364-372.	2.2	34
15	Development of biological macroalgae lignins using copper based metal-organic framework for selective adsorption of cationic dye from mixed dyes. International Journal of Biological Macromolecules, 2020, 165, 2984-2993.	7.5	31
16	Comparison of three different sample preparation procedures for the determination of traffic-related elements in airborne particulate matter collected on glass fiber filters. Talanta, 2012, 88, 689-695.	5.5	30
17	Exploring the structural and optical properties of FeS filled graphene/PVA blend for environmental-friendly applications. Journal of Polymer Research, 2021, 28, 1.	2.4	30
18	Sintering mechanism of blast furnace slag–kaolin ceramics. Materials & Design, 2010, 31, 3677-3682.	5.1	29

#	Article	IF	CITATIONS
19	Determination of rare earth elements in dust deposited on tree leaves from Greater Cairo using inductively coupled plasma mass spectrometry. Environmental Pollution, 2013, 178, 197-201.	7.5	29
20	Effect of annealing temperature on structural and optical properties of gallium oxide thin films deposited by RF-sputtering. Optical and Quantum Electronics, 2020, 52, 1.	3.3	29
21	Influence of the grain size on the quality of standardless WDXRF analysis of river Nile sediments. Microchemical Journal, 2011, 99, 356-363.	4.5	25
22	Correlation between inorganic pollutants in the suspended particulate matter (SPM) and fine particulate matter (PM2.5) collected from industrial and residential areas in GreaterÂCairo, Egypt. Air Quality, Atmosphere and Health, 2019, 12, 241-250.	3.3	25
23	Wavelength dispersive X-ray fluorescence analysis using fundamental parameter approach of Catha edulis and other related plant samples. Spectrochimica Acta, Part B: Atomic Spectroscopy, 2012, 67, 74-78.	2.9	24
24	Characterization and antibacterial capabilities of nanocrystalline CdS thin films prepared by chemical bath deposition. Materials Science in Semiconductor Processing, 2015, 35, 132-138.	4.0	22
25	Comparative elemental analysis of fine particulate matter (PM 2.5) from industrial and residential areas in Greater Cairo-Egypt by means of a multi-secondary target energy dispersive X-ray fluorescence spectrometer. Spectrochimica Acta, Part B: Atomic Spectroscopy, 2018, 145, 29-35.	2.9	21
26	Determination of Cd, Cu, Ni, and Pb in Black Tea from Saudi Arabia using Graphite Furnace Atomic Absorption Spectrometry after Microwave-Assisted Acid Digestion. Analytical Letters, 2013, 46, 2089-2100.	1.8	20
27	Elemental Composition of PM2.5 Aerosol in a Residential–Industrial Area of a Mediterranean Megacity. Archives of Environmental Contamination and Toxicology, 2020, 78, 68-78.	4.1	20
28	Determination of selenium in soil samples using high-resolution continuum source graphite furnace atomic absorption spectrometry and direct solid sample analysis. Analytical Methods, 2014, 6, 2870-2875.	2.7	18
29	Update of photoelectric absorption coefficients in the tables of McMaster. X-Ray Spectrometry, 2006, 35, 52-56.	1.4	15
30	Micro Plasma Generation Using Liquid Sampling-Atmospheric Pressure Glow Discharge. Mikrochimica Acta, 2006, 155, 447-452.	5.0	15
31	Identification of elemental composition of PM _{2.5} collected in Makkah, Saudi Arabia, using EDXRF. X-Ray Spectrometry, 2017, 46, 151-163.	1.4	15
32	EDXRF analysis of suspended particulate matter (SPM) from residential and industrial areas in Cairo, Egypt. X-Ray Spectrometry, 2018, 47, 223-230.	1.4	15
33	Study of half metallic ferromagnetism and thermoelectric properties of spinel chalcogenides BaCr2X4 (X = S, Se, Te) for spintronic and energy harvesting. Journal of Materials Research and Technology, 2022, 18, 2831-2841.	5.8	15
34	Determinations of Sb and Mo in Cairo's dust using high-resolution continuum source graphite furnace atomic absorption spectrometry and direct solid sample analysis. Atmospheric Environment, 2013, 81, 18-24.	4.1	14
35	The role of high-valent (Mo and V) cations in defect spinel iron oxide nanomaterials: Toward improving Li-ion storage. Ceramics International, 2018, 44, 20692-20699.	4.8	14
36	The challenges of Se quantification in bean samples using line and continuum sources atomic absorption spectrometry. Food Chemistry, 2020, 328, 127124.	8.2	13

#	Article	IF	CITATIONS
37	Influence of Niobium Pentoxide Particulates on the Properties of Brushite/Gelatin/Alginate Membranes. Journal of Pharmaceutical Sciences, 2018, 107, 1361-1371.	3.3	11
38	Crystalline <scp>ZnO</scp> and <scp>ZnO</scp> <scp> TiO ₂ </scp> nanoparticles derived from <i>tert</i> â€butyl Nâ€(2 mercaptoethyl)carbamatozinc(<scp>II</scp>) chelate: Electrocatalytic studies for <scp> H ₂ </scp> generation in alkaline electrolytes. International Journal of Energy Research, 2020, 44, 6725-6744.	4.5	11
39	Electron number density and temperature measurements in laser produced brass plasma. EPJ Applied Physics, 2010, 50, 11003.	0.7	10
40	Elucidation of fluorine in SnO2:F sprayed films by different spectroscopic techniques. Journal of Electron Spectroscopy and Related Phenomena, 2012, 185, 140-145.	1.7	10
41	Spectroscopic Characterization of Dust-Fall Samples Collected from Greater Cairo, Egypt. Archives of Environmental Contamination and Toxicology, 2016, 70, 544-555.	4.1	10
42	Synchrotron radiation total reflection X-ray fluorescence (SR-TXRF) and X-ray absorption near edge structure (XANES) of fractionated air particulates collected from Jeddah, Saudi Arabia. Microchemical Journal, 2018, 137, 78-84.	4.5	10
43	Functional properties of quaternary metals (1Ââ^'Âx)ZnMn2O4/(x)MgFe2O4 as supercapacitor electrode. Applied Physics A: Materials Science and Processing, 2021, 127, 1.	2.3	10
44	Lead speciation of PM _{2.5} collected from Greater Cairo, Egypt and Zarqa, Jordan: An energy dispersive Xâ€ray fluorescence and Xâ€ray absorption near edge structure study. X-Ray Spectrometry, 2019, 48, 38-45.	1.4	9
45	Spectroscopic Assessment of Platinum Group Elements of PM10 Particles Sampled in Three Different Areas in Jeddah, Saudi Arabia. International Journal of Environmental Research and Public Health, 2020, 17, 3339.	2.6	9
46	On X-ray tube spectra, the dependence on the angular and electron energy of X-rays from the targets. EPJ Applied Physics, 2007, 37, 291-297.	0.7	8
47	Investigation of structural and optical properties of molybdenum disulfide flakes/polyvinylidene fluoride nanocomposites. Journal of Materials Research and Technology, 2020, 9, 14350-14359.	5.8	8
48	Elemental composition and source apportionment of atmospheric aerosols collected from urban and residential areas of Jordan using multi-secondary targets energy dispersive X-ray fluorescence. Spectrochimica Acta, Part B: Atomic Spectroscopy, 2020, 170, 105900.	2.9	8
49	Optical, structural, and electrical conductivity of PEO/chitosan incorporated by Se NPs produced by one-potential laser ablation. Journal of Materials Science: Materials in Electronics, 2022, 33, 12351-12358.	2.2	8
50	The validity of commercial LIBS for quantitative analysis of brass alloy — comparison of WDXRF and AAS. Journal of Applied Spectroscopy, 2011, 78, 594-600.	0.7	7
51	The role of gas direction in a modified Grimm-type glow discharge for controlling the degree of crystallinity in brass alloy thin films. Vacuum, 2015, 121, 105-112.	3.5	7
52	Levels of Trace Elements in Black Teas Commercialized in Saudi Arabia Using Inductively Coupled Plasma Mass Spectrometry. Biological Trace Element Research, 2016, 174, 477-483.	3.5	7
53	Quantitative elemental analysis and natural radioactivity levels of mud and salt collected from the Dead Sea, Jordan. Microchemical Journal, 2017, 133, 352-357.	4.5	7
54	Applicability of Low-Cost Binders for the Quantitative Elemental Analysis of Urinary Stones Using EDXRF Based on Fundamental Parameter Approach. Biological Trace Element Research, 2020, 195, 417-426.	3.5	7

4

#	Article	IF	CITATIONS
55	Pt–ZnO/M (M = Fe, Co, Ni or Cu): A New Promising Hybrid-Doped Noble Metal/Semiconductor Photocatalysts. Journal of Inorganic and Organometallic Polymers and Materials, 2020, 30, 4627-4636.	3.7	7
56	Influence of argon flow rate on structural and optical properties of transparent Nb2O5 thin films. Optical and Quantum Electronics, 2019, 51, 1.	3.3	6
57	Synthesis and Characterization of Eco-Friendly CMC/Maghemite Nanocomposite Films. Journal of Electronic Materials, 2021, 50, 7098-7109.	2.2	6
58	Gamma radiation introduces improvement in Ac conductivity behavior and dielectric characterization of CuONPs@PVP-PVA nano matrix films prepared by one-potential laser ablation method. Optical and Quantum Electronics, 2022, 54, 1.	3.3	6
59	Sputtered-deposited thin brass films in a modified glow discharge Grimm-type source. EPJ Applied Physics, 2006, 35, 93-105.	0.7	5
60	Molecular imaging of alkaloids in khat (Catha edulis) leaves with MeV-SIMS. Nuclear Instruments & Methods in Physics Research B, 2017, 404, 140-145.	1.4	5
61	Method Development and Quantitative Elemental Analysis of <i>Mentha Longifolia</i> L. Leaves from Saudi Arabia by Total Reflection X-Ray Fluorescence. Analytical Letters, 2018, 51, 1433-1444.	1.8	5
62	Synchrotron X-ray fluorescence and X-ray absorption near edge structure of low concentration arsenic in ambient air particulates. Journal of Analytical Atomic Spectrometry, 2021, 36, 981-992.	3.0	5
63	Spectroscopic Study of Heavy Metals at Different Depths in Southeastern Soil of Nile Delta, Egypt. Spectroscopy Letters, 2011, 44, 186-193.	1.0	4
64	In vitro surface biocompatibility of high-content silicon-substituted calcium phosphate ceramics. Open Chemistry, 2013, 11, 140-150.	1.9	4
65	Spectroscopic Characterization of Urinary Stones Richening with Calcium Oxalate. Biological Trace Element Research, 2021, 199, 2858-2868.	3.5	4
66	<scp>EDXRF</scp> , <scp>FTIR</scp> , and <scp>XRD</scp> characterization of low calcium oxalate urinary stones collected from arid area. X-Ray Spectrometry, 2022, 51, 214-229.	1.4	4
67	Seasonal Variability of Elemental Composition and Phytochemical Analysis of Moringa oleifera Leaves Using Energy-Dispersive X-ray Fluorescence and Other Related Methods. Biological Trace Element Research, 2021, 199, 4319-4329.	3.5	3
68	Direct analysis of essential oils by means of TXRF spectrometry. X-Ray Spectrometry, 2020, 49, 322-331.	1.4	2
69	Ellipsometric study of the optical properties of TlInSeS layered crystal. Optical Materials, 2021, 114, 110958.	3.6	2
70	Bimetallic Nanocomposite of Gold/Silver Scattered in Chitosan via Laser Ablation for Electrical and Antibacterial Utilization. Journal of Electronic Materials, 2022, 51, 3811-3819.	2.2	2
71	Determination of Cu, Zn, and Se in microvolumes of liquid biological samples. Journal of Applied Spectroscopy, 2011, 77, 771-777.	0.7	1
72	Elemental mapping of some collected gold samples from Al-Amar gold mine in Saudi Arabia. Environmental Earth Sciences, 2020, 79, 1.	2.7	0

#	Article	IF	CITATIONS
73	Hydrothermal Synthesis, Anionic Dyes Preconcentration, and Energy Storage of Amino-Functionalized CuNPs Regenerated Chitosan Membrane. Journal of Inorganic and Organometallic Polymers and Materials, 2021, 31, 2492-2500.	3.7	0
74	Magneto-optical effects of MgFe2O4 nanoparticles in solutions and thin films of polystyrene using digital Mach-Zehnder interferometer: An optical based sensor for energy storage controller. Optik, 2021, 242, 167127.	2.9	0